J. Phys. Chem. C **2010,** *114,* 13061–13067

Crystal Grain Orientation in Organic Homo- and Heteroepitaxy of Pentacene and Perfluoropentacene Studied with X-ray Spectromicroscopy

Stefan Kowarik,*,† Katharina Broch,‡ Alexander Hinderhofer,‡ Adam Schwartzberg,§ J. Oriol Ossó,|| David Kilcoyne,⊥ Frank Schreiber,‡ and Stephen R. Leone†,#

Departments of Chemistry and Physics, and Lawrence Berkeley National Laboratory, University of California, Berkeley, California 94720, Institut für Angewandte Physik, Universität Tübingen, 72076 Tübingen, Germany, Molecular Foundry, Lawrence Berkeley National Laboratory, Berkeley, California 94720, MATGAS 2000 A.I.E., Esfera UAB, 08193 Bellaterra, Barcelona, Spain, and Advanced Light Source, Lawrence Berkeley National Laboratory, Berkeley, California 94720

Received: April 25, 2010; Revised Manuscript Received: June 8, 2010

We show that the prototypical p- and n-conducting molecular semiconductors pentacene (PEN) and perfluoropentacene (PFP) exhibit correlated crystal orientation in neighboring grains within a thin film. We use scanning transmission X-ray microscopy (STXM) to measure the film topography in PEN and PFP, and importantly X-ray/optical dichroism also makes it possible to map the grain orientation. PEN exhibits an average grain size of 0.46 ± 0.05 μm^2, but clusters of *aligned* grains are measurably larger at >1.9 μm^2. This finding is rationalized through nucleation of small grains that maintain the epitaxial relation with an underlying larger grain during homoepitaxy. The orientation of PEN grains in (buried) layers of PEN/PFP heterostructures is also assessed with STXM, but no orientational in-plane alignment is found between layers of the two different materials. The findings are important to quantify the number and type of (orientational) grain boundaries for an understanding of charge carrier mobility and exciton diffusion.

I. Introduction

Molecular semiconductor devices have successfully made the transition from basic research to commercial applications such as organic light-emitting diodes (OLEDs) and displays, and next-generation solar cells and transistor circuits will also increasingly rely on organic semiconductors.[1] Significant progress has been made in characterizing the morphology and crystal structure that crucially determine the device performance.[2−5] Yet there are many open questions about the influence of interfaces, lateral grain boundaries, and defect densities on electronic properties of molecular semiconductors. A detailed understanding of the structure−function relationship is important for the improvement of organic devices, which will help to advance the use of polycrystalline layers with better charge carrier mobility than found in the currently prevalent amorphous devices.[4,6]

The two molecules in this study, pentacene (PEN) and the related fluorinated compound perfluoropentacene (PFP), have emerged as benchmark p- and n-conducting semiconductors, respectively.[6−9] The bulk and thin-film crystal structures on silica are known in great detail including interface reconstructions,[6,10−12] and promising charge carrier mobilities of >1 $cm^2\ V^{-1}\ s^{-1}$ (PEN)[13] and 0.024 $cm^2\ V^{-1}\ s^{-1}$ (PFP)[14] have been found. The combination of the two materials is attractive for p−n heterostructures, as the out-of-plane lattice constant of both materials is very similar because both molecules adopt a "standing up" configuration, and therefore the materials are structurally compatible.[15]

While the growth modes and molecular arrangement within the unit cells have been studied in detail, only recently has the in-plane orientation of PEN molecules within individual crystal grains been resolved with transverse shear microscopy (TSM).[16−18] The understanding of the in-plane molecular orientation is important to resolve additional, orientational grain boundaries in islands that would otherwise appear to be a single domain. The charge carrier mobilities and exciton diffusion length will depend on the density of grain boundaries. Apart from the absolute number density, also the type of grain boundary (i.e., low angle boundary < 15°/high angle grain boundary > 15°) will influence the transport processes as a result of the anisotropy in the ionization energies[19] and the anisotropic refractive index.[20] While TSM is able to resolve the angular orientation of domains on the surface of smooth, ultrathin films, for thicker films techniques with bulk sensitivity are advantageous. One such technique is scanning transmission X-ray microscopy (STXM),[21,22] which measures the X-ray absorption of the organic film and is also applicable for buried layers in heterostructures.

In this paper we show that there are clusters of islands with low angle grain boundaries in thick (i.e., ∼60 nm) PEN and PFP films, that is, the in plane molecular/crystalline orientation is correlated between neighboring crystallites. The finding of correlated molecular orientation agrees well with TSM results of large islands in the second PEN monolayer[16] and expands these TSM measurements up to thicker films: additional nucleation from the third, fourth, ... monolayers onward causes a grain size reduction, but those smaller grains that form on top of the second monolayer mostly retain the orientational alignment induced by the second monolayer. While the individual films of PEN and PFP exhibit angular alignment of

* To whom correspondence should be addressed. E-mail: stefan.kowarik@physik.hu-berlin.de. Present address: Institut für Physik, Humboldt Universität zu Berlin, 12489 Berlin, Germany.

† Lawrence Berkeley National Laboratory and University of California, Berkeley.

‡ Universität Tübingen.

§ Molecular Foundry, Lawrence Berkeley National Laboratory.

|| Esfera UAB.

⊥ Advanced Light Source, Lawrence Berkeley National Laboratory.

On appointment as a Miller Research Professor in the Miller Institute for Basic Research in Science.

10.1021/jp103713z © 2010 American Chemical Society
Published on Web 07/09/2010

crystallites, in heterostructures of the two materials we find that no single preferential orientation is induced in the top layer, but the island size is reduced significantly.

II. Experimental Section

Thin films of PEN ($C_{22}H_{14}$, Sigma Aldrich) and PFP ($C_{22}F_{14}$, Kanto Denka Kogyo Co. Ltd., Japan) were prepared by organic molecular beam deposition in ultrahigh vacuum at a base pressure of 5×10^{-10} mbar. As substrates we used amorphous silicon nitride membranes with a thickness of 100 nm (Silson Ltd. Blisworth, U.K.) as received. Crystalline domains in the silicon nitride are smaller than 100 nm, because they would otherwise be visible in transmission electron microscopy (TEM) use of the membranes due to the large silicon nitride lattice constant. We therefore rule out the influence of the silicon nitride on the formation of domains with several micrometers length. As reference substrates, silicon wafers with native oxide were used after sonication in acetone, isopropanol, and Milli-Q water. Single layers and heterostructures were deposited at growth rates of 2.5−3 Å/min and the following substrate temperatures: PEN 28 °C, PFP 50 °C, PEN on PFP 40 °C, PFP on PEN 28 °C, coevaporated 40 °C. Film thicknesses and mixing ratios for coevaporation were determined with a quartz crystal microbalance calibrated separately for PEN and PFP growth through X-ray reflectivity measurements.

For soft X-ray spectroscopy and imaging, we used the STXM at beamline 5.3.2 of the Advanced Light Source, Lawrence Berkeley National Laboratory, Berkeley, CA.[21] In the STXM of carbon C1s transitions, X-rays in the energy range of 280−320 eV are tightly focused on the film surface, and the sample is subsequently raster scanned through the stationary X-ray beam for image acquisition at ∼30 nm spatial resolution. Near-edge X-ray absorption fine structure (NEXAFS)[23] spectra with an energy resolution of ∼200 meV show distinct features for PEN and PFP molecules that enable imaging with chemical contrast, while linear X-ray dichroism makes it possible to study the azimuthal crystal orientation. For spectra and images, the X-ray transmission through the sample is compared to transmission through a blank silicon nitride membrane substrate and converted to optical density (O.D.) according to O.D. $= -\ln(I/I_0)$ where I is the X-ray flux through the sample plus substrate and I_0 is the photon flux through a blank substrate obtained with the same integration and motor-movement times for direct compatibility between I and I_0 (no corrections for the synchrotron ring current are necessary in top-off fill mode). The O.D. at the C1s edge is proportional to the total carbon content (that is, the number of molecules) in the sample, as well as the orientation of the X-ray transition dipole moments of the molecules as detailed below for PEN and PFP X-ray dichroism. When dichroism can be excluded or subtracted from images, the total carbon content in PEN and PFP films is equivalent to the topography of the films in good approximation, because the C-atom density is uniform throughout the crystallites and voids are unlikely due to the "wedding-cake" growth mode of PEN and PFP.

To assess the question of X-ray beam damage after imaging a certain sample area, we directly acquired a larger image containing that area and found no change in O.D. inside and outside the previously imaged area. This demonstrates that, for imaging at a single X-ray energy, the beam-damage influence on STXM images is negligible, a fact further corroborated by the AFM images, which also show the typical topography and monomolecular steps *after* the STXM imaging. When acquiring not only images but spectra with long acquisition times (i.e., repeatedly measuring the same pixel at 50 different energies in an image stack), we could see a "bleached" region with an O.D. decrease of up to 20%. Therefore we limited X-ray exposure times to 1 ms/pixel and energy step so that no change in the PEN samples was visible in the control image. Samples containing PFP were more prone to beam damage, and changes in O.D. of less than 10% had to be tolerated for acquisition of spectra.

Optical microscopy was performed in reflection mode using polarized white light illumination and a 100× objective with N.A. = 0.95. Atomic force microscopy (AFM) images were acquired in air using a Veeco MultiMode AFM in tapping mode.

Statistical analysis of STXM images was performed with the software ImageJ to obtain size distributions of grains and orientational clusters. The size of individual grains was determined by height thresholding in STXM topography images, and the result agreed with grain size analysis of AFM images. Orientational clusters were selected using a brightness threshold to mark 25% of the brightest image area in the X-ray dichroism measurement, that is, clusters with only low angle grain boundaries (orientation of the PEN *a*-axis deviating less than ±15° from horizontal alignment in images) were analyzed to obtain the orientational cluster size. For both AFM and STXM, at least three different spots per sample were imaged, and good consistency between different sample spots was found, that is, the organic films are laterally homogeneous.

III. Results and Discussion

A. PEN. PEN films on Si_3N_4 and SiO_2 substrates were studied by AFM as a reference for STXM measurements and also to establish that the growth on Si_3N_4 is very similar to the growth on well-known silica substrates. The AFM morphology of a 58 nm PEN film in Figure 1a on amorphous Si_3N_4 (surface energy 46.1 mJ/m^2)[24] is very similar to the one on amorphous SiO_2 (40.1 mJ/m^2)[24] processed in parallel with the Si_3N_4 membranes. Molecular terraces with a monomolecular step height of approximately 1.5−2.0 nm are visible on PEN islands, demonstrating that the molecules in the film are oriented in the standing upright orientation commonly found on inert substrates.[11] Also the nucleation density of $\sim 1.0\ \mu m^{-2}$ in the first PEN monolayer on Si_3N_4 (AFM images not shown) is very similar to the nucleation density of $\sim 0.7\ \mu m^{-2}$ found for room temperature growth on silicon.[25] Comparing an AFM image with a STXM image of the same sample area (see Figure 1a,b) the same islands seen in the AFM topography can also clearly be discerned in the STXM image, but the STXM contrast is different as the total X-ray absorption is dependent on the surface topography as well as the orientation of the dichroic PEN crystallites. This sensitivity to molecular in-plane orientation makes it possible to detect orientational grain boundaries that would be missed in AFM images (see arrows in Figure 1a,b).

To understand the origin of the STXM contrast in dichroic PEN films we consider the molecular arrangement as schematically pictured in Figure 1 c. PEN crystallites have been found to exhibit nearly identical unit cell dimensions and molecular orientation with herringbone angles between 54 −59° on a range of inert substrates.[11] Therefore we use the molecular arrangement on amorphous SiO_2 as a reasonable approximation for the unknown PEN thin film crystal structure on Si_3N_4. The molecular herringbone angle projected into the substrate plane leads to an angle of ∼54° between the carbon 1s−π* transition dipoles of the two molecules within a unit cell. Using a $\cos^2$

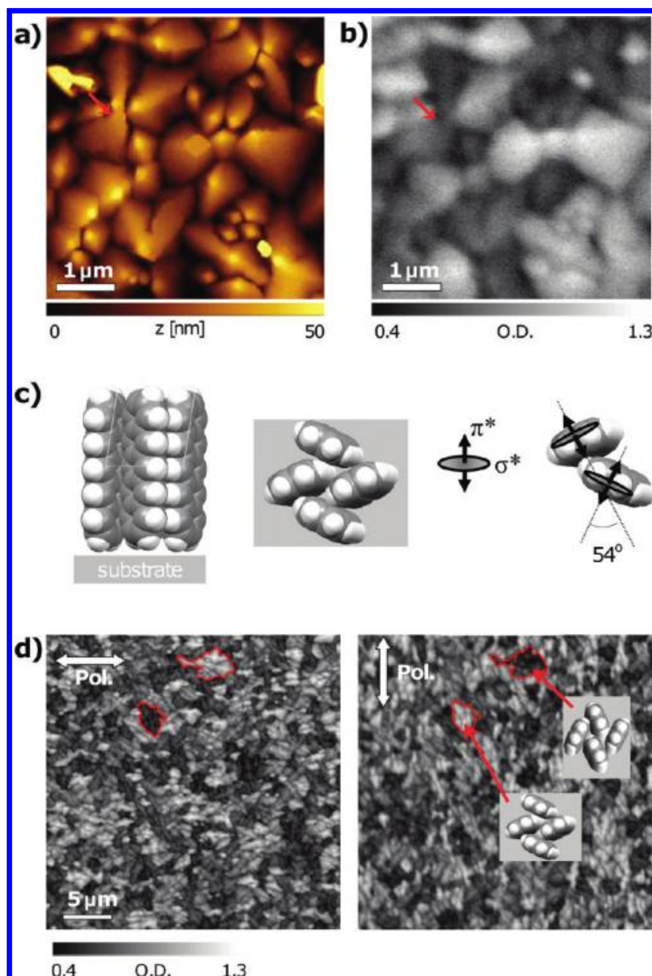

Figure 1. (a) AFM image of a 58 nm thick PEN film on amorphous Si_3N_4 showing the topography including terraces with monomolecular height. (b) STXM image of the same sample area acquired at an X-ray energy of 285.6 eV (PEN π^* transition) showing contrast due to both topography and molecular orientation. Arrow: Orientational grain boundaries are easily detected in STXM but hard to observe in the AFM topography. (c) Schematic of the molecular arrangement in PEN thin film. For the herringbone angle of 54° between the two molecules within the unit cell, the combined π^* absorption is stronger in the vertical than in the horizontal direction, leading to X-ray dichroism. (d) The contrast due to dichroism reverses upon rotating the X-ray polarization. The molecular orientation as deduced from the linear dichroism is exemplarily given for two clusters.

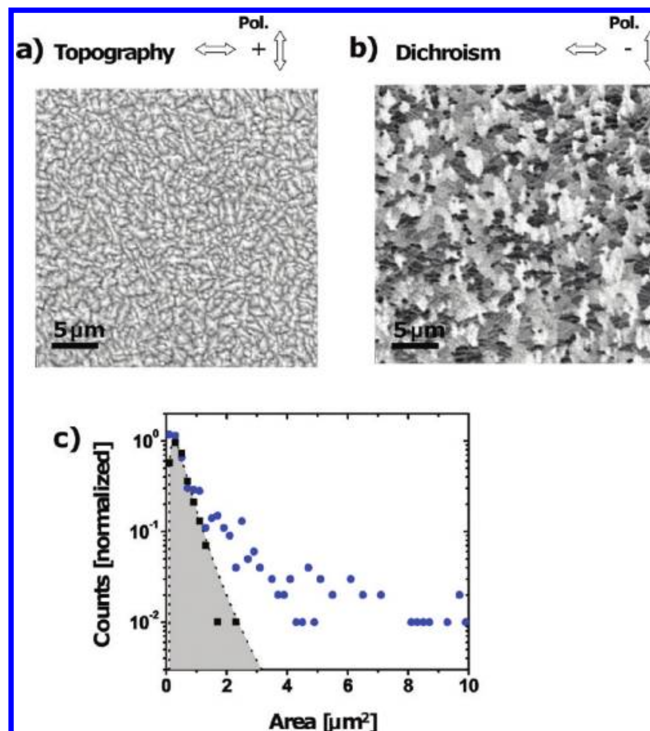

Figure 2. (a) STXM topography image showing individual PEN crystallites (addition of two STXM images in Figure 1d). (b) STXM linear dichroism image (subtracted images in Figure 1d) showing crystallite angular orientation as a contrast revealing island clusters with aligned orientation. (c) The size histogram shows that individual crystallites in panel a have an average area of 0.46 μm^2 (gray shaded area is a log-normal fit to the histogram), while the average cluster size in panel b is 1.9 μm^2.

angular dependence of the transition dipole of the individual molecule, the 1s$-\pi^*$ absorption of a crystal is calculated to be 70% weaker for horizontal X-ray polarization as compared to vertical polarization for a crystallite orientation as shown in Figure 1 c. As a result, the absorption contrast in STXM images is not only (trivially) modulated by the film thickness d according to Beer's law $e^{-\alpha d}$ but also strongly influenced by molecular orientation. Indeed, by changing the X-ray polarization, we observe a contrast reversal (see Figure 1 d) confirming the X-ray dichroism/azimuthal molecular orientation as a dominant contrast mechanism in STXM images of PEN. From the observed dichroism, the molecular orientation can therefore be deduced as shown for the outlined PEN island clusters in the inset of Figure 1 d.

Using the STXM images at two different incident polarizations, it is possible to separate the contribution of the PEN topography and the contrast due to molecular orientation as shown in Figure 2. The addition of two images acquired at perpendicular polarization yields the averaged absorption, which is only proportional to the sample thickness and clearly shows the PEN mound topography consisting of many small islands (Figure 2a). Subtracting the two images as shown in Figure 2b yields only the linear dichroism of the sample and therefore provides a map of the crystallite orientation with an angular resolution of better than ±15°. Interestingly, the regions of similar orientation with only low angle grain boundaries within this orientational map are considerably larger than the individual islands observed in the topography.

This clustering of islands with correlated molecular orientation is quantified in Figure 2c, which shows the size distribution of individual islands and correlated clusters (statistics for ~150 islands and 50 clusters shown). From the island size histogram and its log-normal fit we determine the average size of individual PEN islands in the STXM image to be 0.46 ± 0.05 μm^2 (throughout this paper, numbers given are total areas, the characteristic island radius is $(0.46/\pi)^{1/2}$), that is, the island size in thick films is smaller than the island size of 1.0 μm^2 in the first monolayer. By contrast, the size histogram for orientational clusters is skewed to larger island sizes with an average size of 1.9 μm^2. This shows that, on average, an orientational domain likely consists of more than four islands, and the compact shapes indicate that, during growth, the orientation of PEN islands is correlated with neighboring islands. We note that, in ref 26, microelectron diffraction with 3 μm resolution also showed large orientational domains greater than 30 μm^2 for PEN growth at 85 °C, while, for room temperature growth similar to this study, no domains could be observed. This discrepancy at room temperature is due to the limited resolution in ref 26 and serves to show the superior spatial resolution of the STXM for imaging grain orientation.

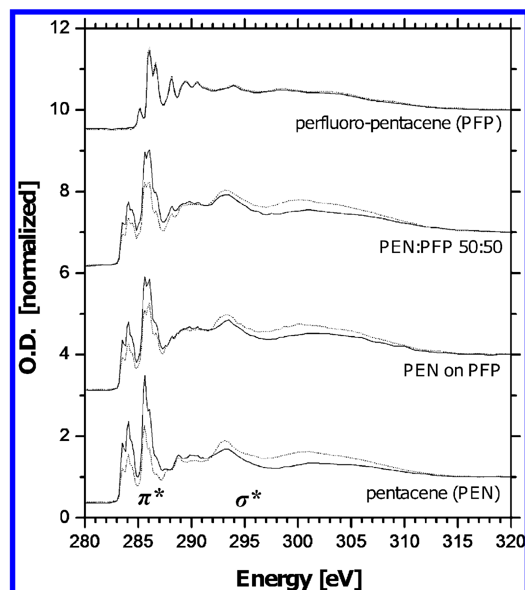

Figure 3. Comparison of the micro-NEXAFS spectra of a bilayer, coevaporated, and pure thin films of PEN and PFP (normalized at 320 eV). Spectra with the lowest (dotted line) and highest (solid line) absorption in the π^* region are shown. Films that contain PEN show dichroism, i.e., the absorption in the π^* region depends on the grain orientation. For strong π^* absorption, the σ^* absorption is weak and vice versa, as expected. In contrast to PEN, for PFP we find no spectral variation within an image, as PFP only shows topographical contrast and no X-ray dichroism.

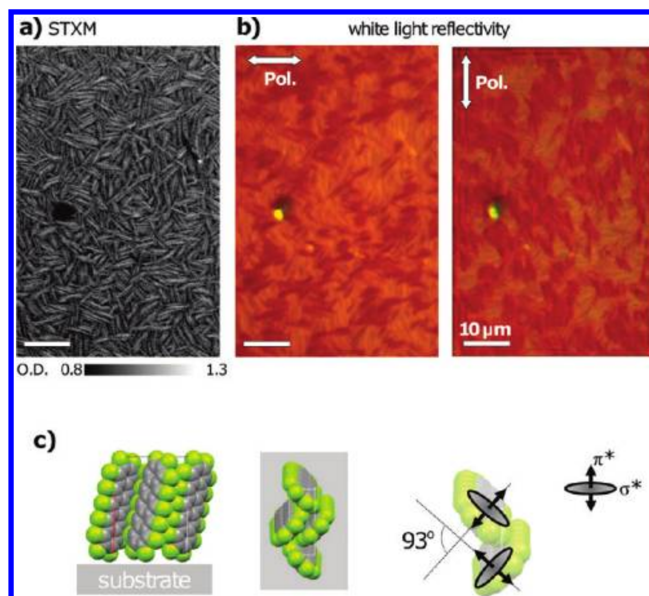

Figure 4. (a) STXM image (286.1 eV) of a 65 nm PFP thin film on silicon nitride showing the needle-like morphology also observed for PFP growth on silicon oxide.[29] (b) While no dichroism is visible in STXM, the same sample area shows pronounced dichroism in polarized white light microscopy. (c) Schematic of the molecular arrangement in PFP films. No X-ray dichroism is observed, as the angle between the π^* transitions of the two molecules in the unit cell is close to 90°.

In conclusion we find that the average crystal grain area evolves from 1.0 μm^2 in the first monolayer to a size of 0.46 μm^2 in a 58 nm thick PEN film, while orientationally correlated PEN clusters with an average area of 1.9 μm^2 (in a 58 nm thick film) are larger than individual grains both in the first monolayer and thick films. A possible explanation for the surprising finding of correlated clusters being larger than the island size in the beginning of growth can be found in TSM studies, which show the second monolayer growing in larger oriented domains compared to the first monolayer.[16,18] These second monolayer islands have a size of >3 μm^2, which serves to explain the size we find in oriented clusters.[18] To summarize the growth, we find that, following the unusual homoepitaxy of large PEN islands in the first and second monolayer, (i) the PEN island size decreases through additional nucleation, and (ii) the smaller grains largely maintain the orientation induced by the second monolayer leading to orientational correlation between grains.

For a more detailed characterization of the PEN dichroism, we have used the spectromicroscopy capability in STXM to acquire micro-NEXAFS spectra from differently oriented PEN islands as shown in Figure 3. The energetic position of π^* excitations in the region below 290 eV and several broad σ^* transitions at higher energies agree well with previously published values, and we refer to the experimental and theoretical studies[27,28] for the detailed assignment of transition energies. As expected, the strength of the transitions into empty σ^* orbitals decreases for increasing absorption in the π^* region because the orbitals are orthogonal to each other (see Figure 1c). In comparison to previous studies we find the π^* absorption peak to be stronger with respect to the σ^* absorption (solid line in Figure 3), because the micro-NEXAFS does not average the spectra of crystallites with different azimuthal orientation.[28] Experimentally, we find the contrast between high and low absorption in the π^* region to be 35 ± 5% as compared to the theoretically expected 70%. We attribute this reduced experimental contrast to the fact that only a small sampling size of ~20 PEN islands was measured with full spectroscopic information, and therefore islands aligned exactly along horizontal and vertical X-ray orientation may not be present in the sample, leading to lower observed dichroic contrast. Additionally noncommensurate homoepitaxy of PEN as found between the first and second monolayers will lower the experimentally observed dichroism.

B. PFP. For PFP films, we also find that neighboring crystallites often are orientationally aligned, as evidenced by the frequent parallel orientation of needle-shaped PFP crystallites. Figure 4a shows a STXM image of a 65 nm film PFP grown on silicon nitride, and characteristic elongated crystallites are also observed for growth on silicon oxide.[29] The image contrast for PFP is weaker than for PEN, because it is solely due to thickness variations (topographical contrast), and PFP spectra do not exhibit dichroism, i.e., the spectra of dark and light image regions are identical (see Figure 3). The clusters of orientationally aligned PFP crystallites become more obvious when imaging the same sample area in polarized light microscopy, which shows distinct optical dichroism in true color images in Figure 4b. While twin growth can lead to an orientational correlation between two crystallites, we also find larger clusters consisting of three and more oriented needles. The simplest explanation for this is a mechanism in which the first substrate wetting monolayer forms large oriented domains and thereby determines the orientation of several smaller crystallites in further homoepitaxial growth on top of it. Additional TSM studies of the first PFP monolayer are needed to confirm this hypothesis. Comparing STXM and optical images, we further find that individual crystallites always consist of a single domain, that is, there are no orientational grain boundaries within a PFP island.

To understand the vanishing X-ray dichroism in PFP, the thin film crystal structure is shown in Figure 4c; again, we approximate the unknown structure on silicon nitride with the one

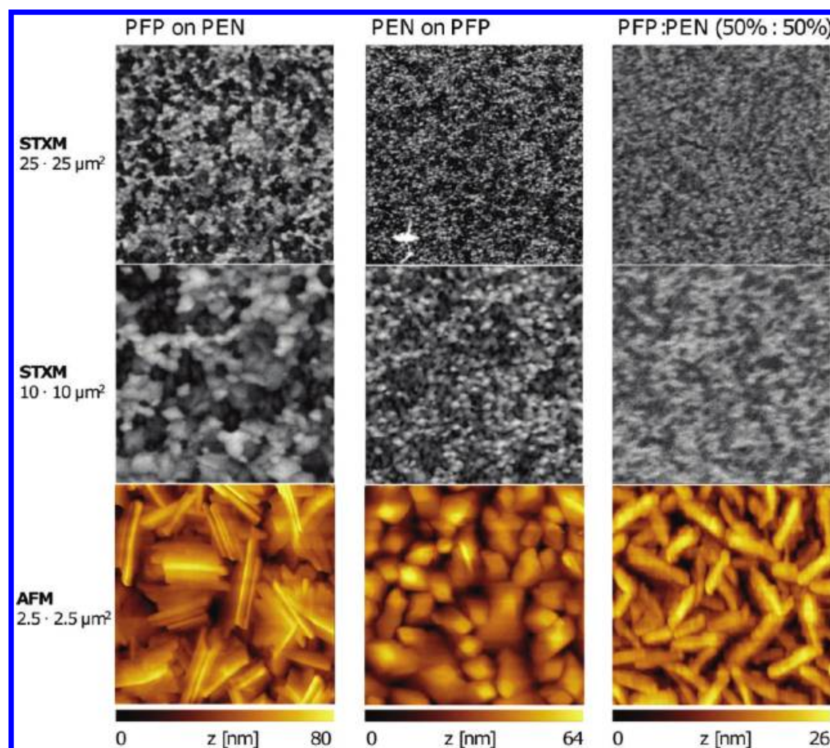

Figure 5. Comparison of STXM and AFM images of heterostructures of PFP on PEN (29 on 58 nm), PEN on PFP (58 on 30 nm), and a coevaporated film of PEN:PFP (50%:50%, 60 nm total thickness). The contrast in the bilayers is dominated by dichroism in PEN layers. For PFP on PEN we find that the morphology of the PEN layer is very similar to the individual layer, as seen in STXM images, while the AFM reveals typical elongated PFP crystallites on top of the PEN islands. For growth of PEN on PFP, the island sizes are significantly reduced. The mixture of molecules in a coevaporated film forms a new crystal structure with slightly elongated crystals. No phase separation between PEN and PFP is visible down to a resolution of 75 nm. The O.D. scale of all STXM images has been normalized to account for differences in film thickness and to allow for a direct comparison.

on silicon oxide. The π^*-transition dipoles of the two molecules within the unit cell form an angle of ~93° when projected into the sample plane. This explains the negligible X-ray dichroism in PFP, because the corresponding $\cos^2$ and $\sin^2$ absorption characteristics of the two molecules nearly cancel each other, and therefore the C1s$-\pi^*$ absorption is isotropic. The same reasoning can be applied to optical transitions along the short axis of the molecule and perpendicular to the molecular plane, but surprisingly, in optical microscopy, distinct dichroism is visible (for PEN we find the situation to be reversed with strong X-ray and weak optical dichroism). The linear dichroism in the visible region can be attributed to greater sensitivity in light microscopy and also to optical transitions along the long axis of the molecule,[20] which is tilted more from the 'standing upright' orientation than PEN. A quantification of the optical dichroism is difficult though, because absorption as well as the surface reflection and its interference with the backside reflection influence the observed contrast (with an X-ray reflectivity of 3×10^{-9}, the problem of a backside reflection does not occur for X-ray dichroism). Indeed the optical dichroism is only clearly visible for samples on a 100 nm thick membrane and is weak on silicon-supported Si_3N_4, demonstrating that the backside reflection leads to enhanced contrast.

Comparing the PFP NEXAFS spectrum in Figure 3 to the PEN spectrum, we find a significant shift of the most prominent π^* resonance from 285.6 eV for PEN to 286.1 eV for PFP. This is an effect commonly observed for fluorination, as the C1s core electron binding energy increases for (partially) fluorinated fullerenes,[30] and our measurements are also further sensitive to changes in the π^* and σ^* orbitals.

C. Heterostructures. Having characterized the individual layers of PEN and PFP, we now turn to bilayers and coevaporated films of the two compounds to investigate whether the orientational correlations also extend beyond the interface of the two materials through epitaxial relations in these heterostructures. Figure 5 shows a comparison of STXM and AFM images of three heterostructures: PFP on PEN (29 on 58 nm), PEN on PFP (58 on 30 nm), and a coevaporated film of PEN:PFP (50%:50%, 60 nm total thickness).

For growth of PFP on PEN, we find that the island size of PFP is greatly reduced from a length of more than 5 μm to less than 1 μm because the PFP crystallites grow in a shape and size similar to the underlying PEN islands. The AFM image still shows needle-like growth on top of individual PEN layers, but several orientations of these needles on a single PEN island indicate that there is either coexistence of several epitaxial coincidence types or no epitaxial relation at all between the two materials, which is not surprising as the in-plane unit cells of PEN (a = 5.96 Å, b = 7.60 Å)[11] and PFP (b = 4.53 Å, c = 11.4 Å)[29] are very different. The STXM image contrast in the bilayer sample is dominated by dichroism in PEN layers, i.e., the STXM images give information about the buried PEN film structure, and the thin PFP layer does contribute less than 20% to the observed contrast (PEN: ΔO.D. = 0.9, from Figure 1d; PFP: ΔO.D. < 0.2 for 29 nm PFP, see Figure 4a). Not surprisingly, the PEN layer underneath the PFP film shows no change in island size, and orientational clusters are unchanged compared to Figure 1.

Similar to the bilayer PFP on PEN, the reverse structure of PEN on PFP also shows a distinct reduction of PEN island area from 0.46 ± 0.05 μm^2 in a pure PEN layer to an average island area of 0.07 ± 0.01 μm^2 in the heterostructure. The STXM image contrast is still dominated by linear dichroism of PEN, but the contrast observed in the bilayer spectra in Figure 3 is

reduced due to increased disorder/stacking of different PEN island orientations. Some faint correlation of PEN island orientation is visible in small orientational clusters, but no orientational correlation on the length scale of the underlying several micrometer long PFP crystallites is visible. This shows that no long-range epitaxial relation of PEN on PFP is formed in this heterostructure.

For the coevaporated sample, we observe complete mixing of the two types of molecules, and a different island morphology with an average island area of $0.10 \pm 0.01\ \mu m^2$. We have fitted the spectra of pure PEN and PFP to image stacks (i.e., images with full spectral information at every pixel), but within our sensitivity (20% enrichment of one material could be detected) we do not find any phase separation of PEN and PFP domains down to an image resolution of 75 nm. This agrees with previous results of IR measurements that demonstrate mixing on the molecular scale with one PFP and one PEN molecule per unit cell.[15] The STXM images and spectra in Figure 3 show that the mixed crystal exhibits dichroism, but the contrast is weak for the coevaporated sample. Comparing STXM with the AFM images, the reduced contrast can be explained by stacking of differently oriented crystallites and possibly also decreased dichroism of the new crystal structure in which PFP and PEN are intercalated.

Conclusions

We have shown that STXM microscopy can be used to resolve the topography of thin films of the benchmark p- and n-conducting organic semiconductors PEN and PFP at high resolution. Importantly, STXM of PEN samples also reveals the in-plane molecular orientation of PEN grains through X-ray linear dichroism. The X-ray dichroism in PEN (and the lack thereof in PFP) can be explained by the molecular arrangement within the unit cells, and the respective molecular orientation of PEN grains can be deduced from STXM images. While PFP exhibits essentially no X-ray dichroism, its linear dichroism in the visible range again enables us to image the grain orientation in PFP films. For both PEN and PFP we find that the orientations of neighboring islands are correlated, and larger clusters of islands with similar orientation or low-angle grain boundaries form during growth. This can be explained by multiple nucleations of small islands on top of larger islands in the first and second monolayer, but importantly, the orientation induced by the underlying island is maintained also in thick films.

In contrast to the homoepitaxial growth where the orientation of underlying layers is mostly maintained, we find no orientational domains in PEN/PFP heterostructures. Neither growth of PFP on PEN nor the reverse structure exhibit a single preferential orientation induced by the bottom layer in the top layer. We further find that the island size in heterostructures is strongly decreased in both PEN and PFP top layers. Compared with a single PEN layer, we find that the island area of PEN decreases markedly from $0.46 \pm 0.05\ \mu m^2$ to $0.07 \pm 0.01\ \mu m^2$ when grown on PFP.

These findings show that STXM is a suitable tool to reveal orientational grain boundaries that can be hard to detect with techniques such as AFM. Beyond establishing an absolute number of the average island area and therefore grain boundaries, orientational grain mapping also makes it possible to distinguish between high-angle and low-angle grain boundaries, thereby giving valuable insight into the number and type of imperfections that can impede charge carrier mobility and exciton diffusion. This enables a better understanding of the structure function relationship in organic semiconductors and therefore will help to rationally design improved devices.

Note Added in Proof. After submission of this manuscript two papers on X-ray microscopy investigations of PEN transistors have appeared.[31,32] Their results for PEN transistors agree with our findings on PEN films, but note that the terminology in reference 31 is different because the entire cluster of orientationally aligned islands is called a “grain”.

Acknowledgment. This research is supported by the Deutsche Forschungsgemeinschaft SCHR 700/13-1 and SCHR 700/9-1 (K.B., A.H., and F.S.) and by a postdoctoral fellowship of the Alexander von Humboldt Foundation (S.K.). The salary of S.K. is partially supported by the NSF ERC for Extreme Ultraviolet Science and Technology (No. EEC-0310717). J.O.O. is supported by the Catalan government through the ICREA JE program. At the Advanced Light Source, D.K., A.S., and S.R.L. are supported by the Director, Office of Science, Office of Basic Energy Sciences, U.S. Department of Energy, under Contract No. DE-AC02-05CH11231.

References and Notes

(1) Walzer, K.; Maennig, B.; Pfeiffer, M.; Leo, K. Highly efficient organic devices based on electrically doped transport layers. *Chem. Rev.* **2007**, *107* (4), 1233–1271.

(2) Witte, G.; Wöll, C. Growth of aromatic molecules on solid substrates for applications in organic electronics. *J. Mater. Res.* **2004**, *19* (7), 1889–1916.

(3) Kowarik, S.; Gerlach, A.; Schreiber, F. Organic molecular beam deposition: Fundamentals, growth dynamics, and in situ studies. *J. Phys.: Condens. Matter* **2008**, *20* (18), 184005.

(4) Karl, N. Organic Electronic Materials. In *Organic Electronic Materials*; Farchioni, R.; Grosso, G., Eds.; Springer: Berlin, 2001; Vol. II.

(5) Schreiber, F. Organic molecular beam deposition: Growth studies beyond the first monolayer. *Phys. Status Solidi A: Appl. Res.* **2004**, *201* (6), 1037–1054.

(6) Mannsfeld, S. C. B.; Virkar, A.; Reese, C.; Toney, M. F.; Bao, Z. Precise structure of pentacene monolayers on amorphous silicon oxide and relation to charge transport. *Adv. Mater.* **2009**, *21* (22), 2294–2298.

(7) Nickel, B.; Fiebig, M.; Schiefer, S.; Goellner, M.; Huth, M.; Erlen, C.; Lugli, P. Pentacene devices: Molecular structure, charge transport and photo response. *Phys. Status Solidi A: Appl. Mater. Sci.* **2008**, *205* (3), 526–533.

(8) Sakamoto, Y.; Suzuki, T.; Kobayashi, M.; Gao, Y.; Fukai, Y.; Inoue, Y.; Sato, F.; Tokito, S. Perfluoropentacene: High-performance p−n junctions and complementary circuits with pentacene. *J. Am. Chem. Soc.* **2004**, *126* (26), 8138–8140.

(9) Koch, N.; Vollmer, A.; Duhm, S.; Sakamoto, Y.; Suzuki, T. The effect of fluorination on pentacene/gold interface energetics and charge reorganization energy. *Adv. Mater.* **2007**, *19* (1), 112.

(10) Ruiz, R.; Choudhary, D.; Nickel, B.; Toccoli, T.; Chang, K.-C.; Mayer, A. C.; Clancy, P.; Blakely, J. M.; Headrick, R. L.; Iannotta, S.; Malliaras, G. G. Pentacene thin film growth. *Chem. Mater.* **2004**, *16*, 4497–4508.

(11) Schiefer, S.; Huth, M.; Dobrinevski, A.; Nickel, B. Determination of the crystal structure of substrate-induced pentacene polymorphs in fiber structured thin films. *J. Am. Chem. Soc.* **2007**, *129*, 10316–10317.

(12) Yoshida, H.; Inaba, K.; Sato, N. X-ray diffraction reciprocal space mapping study of the thin film phase of pentacene. *Appl. Phys. Lett.* **2007**, *90* (18), 181930–181933.

(13) Nelson, S. F.; Lin, Y. Y.; Gundlach, D. J.; Jackson, T. N. Temperature-independent transport in high-mobility pentacene transistors. *Appl. Phys. Lett.* **1998**, *72* (15), 1854–1856.

(14) Sakamoto, Y.; Suzuki, T.; Kobayashi, M.; Gao, Y.; Inoue, Y.; Tokito, S. Perfluoropentacene and perfluorotetracene: Syntheses, crystal structures, and FET characteristics. *Mol. Cryst. Liq. Cryst.* **2006**, *444*, 225–232.

(15) Salzmann, I.; Duhm, S.; Heimel, G.; Rabe, J. P.; Koch, N.; Oehzelt, M.; Sakamoto, Y.; Suzuki, T. Structural order in perfluoropentacene thin films and heterostructures with pentacene. *Langmuir* **2008**, *24* (14), 7294–7298.

(16) Kalihari, V.; Ellison, D. J.; Haugstad, G.; Frisbie, C. D. Observation of unusual homoepitaxy in ultrathin pentacene films and correlation with surface electrostatic potential. *Adv. Mater.* **2009**, *21* (30), 3092–3098.

(17) Kalihari, V.; Tadmor, E. B.; Haugstad, G.; Frisbie, C. D. Grain orientation mapping of polycrystalline organic semiconductor films by transverse shear microscopy. *Adv. Mater.* **2008**, *20* (21), 4033–4039.

(18) Zhang, J.; Rabe, J. P.; Koch, N. Grain-boundary evolution in a pentacene monolayer. *Adv. Mater.* **2008**, *20* (17), 3254–3257.

(19) Duhm, S.; Heimel, G.; Salzmann, I.; Glowatzki, H.; Johnson, R. L.; Vollmer, A.; Rabe, J. P.; Koch, N. Orientation-dependent ionization energies and interface dipoles in ordered molecular assemblies. *Nat. Mater.* **2008**, *7* (4), 326–332.

(20) Hinderhofer, A.; Heinemeyer, U.; Gerlach, A.; Kowarik, S.; Jacobs, R. M. J.; Sakamoto, Y.; Suzuki, T.; Schreiber, F. Optical properties of pentacene and perfluoropentacene thin films. *J. Chem. Phys.* **2007**, *127* (19), 194705.

(21) Kilcoyne, A. L. D.; Tyliszczak, T.; Steele, W. F.; Fakra, S.; Hitchcock, P.; Franck, K.; Anderson, E.; Harteneck, B.; Rightor, E. G.; Mitchell, G. E.; Hitchcock, A. P.; Yang, L.; Warwick, T.; Ade, H. Interferometer-controlled scanning transmission X-ray microscopes at the Advanced Light Source. *J. Synchrotron Radiat.* **2003**, *10*, 125.

(22) R, H. Fink; Hub, C.; Tzvetkov, G. Zone-plate based nanospectroscopy with soft X-rays at the SLS. *Acta Phys. Pol., A* **2009**, *115*, 462.

(23) Stöhr, J. *NEXAFS Spectroscopy*, 2nd ed.; Springer-Verlag: Berlin/Heidelberg/New York, 2003.

(24) Miskiewicz, P.; Kotarba, S.; Jung, J.; Marszalek, T.; Mas-Torrent, M.; Gomar-Nadal, E.; Amabilino, D. B.; Rovira, C.; Veciana, J.; Maniukiewicz, W.; Ulanski, J. Influence of SiO_2 surface energy on the performance of organic field effect transistors based on highly oriented, zone-cast layers of a tetrathiafulvalene derivative. *J. Appl. Phys.* **2008**, *104* (5), 054509–4.

(25) Ruiz, R.; Nickel, B.; Koch, N.; Feldman, L. C.; Haglund, R. F.; Kahn, A.; Scoles, G. Pentacene ultrathin film formation on reduced and oxidized Si surfaces. *Phys. Rev. B* **2003**, *67* (12), art. no. 125406.

(26) Laquindanum, J. G.; Katz, H. E.; Lovinger, A. J.; Dodabalapur, A. Morphological origin of high mobility in pentacene thin-film transistors. *Chem. Mater.* **1996**, *8* (11), 2542–2544.

(27) Alagia, M.; Baldacchini, C.; Betti, M. G.; Bussolotti, F.; Carravetta, V.; Ekstrom, U.; Mariani, C.; Stranges, S. Core−shell photoabsorption and photoelectron spectra of gas-phase pentacene: Experiment and theory. *J. Chem. Phys.* **2005**, *122* (12), 124305–6.

(28) Käfer, D.; Witte, G. Evolution of pentacene films on Ag(1 1 1): Growth beyond the first monolayer. *Chem. Phys. Lett.* **2007**, *442* (4−6), 376–383.

(29) Kowarik, S.; Gerlach, A.; Hinderhofer, A.; Milita, S.; Borgatti, F.; Zontone, F.; Suzuki, T.; Biscarini, F.; Schreiber, F. Structure, morphology, and growth dynamics of perfluoro-pentacene thin films. *Phys. Status Solidi RRL: Rapid Res. Lett.* **2008**, *2* (3), 120–122.

(30) Mikoushkin, V.; Shnitov, V.; Bryzgalov, V.; Gordeev, Y.; Boltalina, O.; Goldt, I.; Molodtsov, S.; Vyalikh, D. Core electron level structure in C60F18 and C60F36 fluorinated fullerenes. *Tech. Phys. Lett.* **2009**, *35* (3), 256–259.

(31) Bräuer, B.; Virkar, A.; Mannsfeld, S. B. C.; Bernstein, D. P.; Kukreja, R.; Chou, K. W.; Tyliszczak, T.; Bao, Z. Acremann, Y. X-ray Microscopy Imaging of the Grain Orientation in a Pentacene Field-Effect Transistor. *Chem. Mater.* **2010**, *22* (12), 3693–3697.

(32) Hub, C.; Burkhardt, M.; Halik, M.; Tzvetkov, G.; Fink, R. In situ STXM Investigations of Pentacene-based OFETs during Operation. *J. Mater. Chem.* **2010**, *20* (23), 4884–4887.

JP103713Z